ELSEVIER

International Journal of Minerals, Metallurgy and Materials
Volume 16, Number 1, February 2009, Page 25

Metallurgy

Characteristics of shell thickness in a slab continuous casting mold

Di-feng Wu[1)], *Shu-sen Cheng*[1)], *and Zi-jian Cheng*[2)]

1) School of Metallurgical and Ecological Engineering, University of Science and Technology Beijing, Beijing 100083, China

2) Steelmaking Plant, Jiuquan Iron and Steel Co. Ltd., Jiayuguan 735100, China

(Received 2008-02-06)

Abstract: The key to reduce shell breakout in the continuous casting process is to control shell thickness in the mold. A numerical simulation on the turbulent flow and heat transfer coupled with solidification in the slab mold using the volume of fluid (VOF) model and the enthalpy-porosity scheme was conducted and the emphasis was put upon the flow effect on the shell thickness profiles in longitudinal and transverse directions. The results show that the jet acts a stronger impingement on the shell of narrow face, which causes a zero-increase of shell thickness in a certain range near the impingement point. The thinnest shell on the slab cross-section locates primarily in the center of the narrow face, and secondly near the corner of the wide face. Nozzle optimization can obviously increase the shell thickness and make it more uniform.

Key words: continuous casting; slab mold; shell thickness; nozzle optimization

[*This work was financially supported by the National Natural Science Foundation of China (No.60672145).*]

1. Introduction

It is of great importance to form a thick and sufficiently uniform solidifying shell in the mold to prevent breakout in the continuous casting process. Breakout starts to take place at the thinnest point commonly, and therefore, it is significant to investigate the slab thickness distribution in longitudinal and transverse directions to determine this point. Experimental and numerical simulations are the two ways for the measurement of shell thickness in the mold. The former such as adding sulfur into the mold [1], disturbs the normal production and obtains some useful data, which cannot characterize the shell thickness profiles thoroughly. On the other hand, several scholars have researched the flow, heat transfer, and solidification in the mold by numerical simulation [2-5]. However, some profound researches on the characteristics of the shell thickness have been done.

The jet delivering from the nozzle acts a strong impingement on the shell, and therefore, the heat transfer and solidification in the mold are associated with the flow pattern closely. A proper flow causing weaker impingement on the shell can promote a more uniform and thicker shell, which has the same purpose for using the submerged entry nozzle (SEN) with rotational flow guide device [6] or electromagnetic brake [7-8] in the continuous casting process. Furthermore, as the flow source in the mold, SEN influences the flow and heat transfer patterns greatly. Consequently, the optimization for nozzle design can improve the shell thickness distribution.

A numerical simulation on the turbulent flow and heat transfer coupled with solidification in the slab mold was conducted in this article and the emphasis was put upon the flow effect on the shell thickness profiles in longitudinal and transverse directions. The nozzle was also optimized to increase the shell thickness.

2. Physical and mathematical model

2.1. Physical model

A series of complicated phenomena take place in the continuous casting process such as turbulent flow, heat transfer, solidification, and solute segregation, in which flow and solidification are the basic phenomena. Taking all these phenomena into account in the model

Corresponding author: Di-feng Wu, **E-mail:** wudifeng_0121083@163.com

Also available online at www.sciencedirect.com

is impossible. By appropriately simplifying the model, the present study puts the emphasis upon the flow and heat transfer in mold cavity, especially on the solidifying shell profile. The assumptions in the model are given as follows.

(1) The flow and heat transfer are twofold symmetrical, therefore, only one quarter of the mold needs to be modeled.

(2) The effects of the mold oscillation and the taper of the mold walls are not taken into consideration.

(3) Ignoring the effect of the protective flux layer, the interface of steel and air is treated as the free surface.

(4) The density of the liquid steel is constant regardless of the natural convection in molten pool because of the temperature difference.

The basic simulation conditions for slab casting are summarized in Table 1.

Table 1. Simulation conditions for slab casting

Slab thickness	220 mm
Slab width	1550 mm
Mold length	900 mm
SEN bore diameter	60 mm
Nozzle port size (width×height)	45 mm×75 mm
SEN submergence depth	150 mm
Nozzle port angle	Downward 15°
Casting speed	1.0 m/min
Casting temperature	1540°C
Heat transfer coefficient at narrow face	1069 W/(m^2·°C)
Heat transfer coefficient at wide face	975 W/(m^2·°C)

2.2. Mathematical model

The present model takes the flow of molten steel in the mold as a 3-dimensional steady-state multiphase flow with solidification. The volume of fluid (VOF) model [9] can model two or more immiscible fluids by solving a single set of momentum equations and tracking the volume fraction of each of the fluids throughout the computational domain. Ignoring the flux layer, there is an obvious interface between air and steel, where the VOF model is competent to track the wave. The standard two-equation k-ε model is chosen to describe the turbulence flow [10-11]. Instead of tracking the liquid-solid front explicitly, the present model uses an enthalpy-porosity formulation [12-13] to characterize the mushy zone flow because of the solidification. The liquid-solid mushy zone is treated as a porous zone with porosity equal to the liquid fraction, and appropriate momentum sink terms are added to the momentum equations to account for the pressure drop caused by the presence of solid steel.

The schematic model of the slab mold is shown in Fig. 1. Taking the symmetrical center of the air outlet plane as the origin, and the slab width-, thickness-, and height-directions as the x-, y-, and z-directions, respectively, we build a Cartesian coordinate system. As we know, two large recirculation flows exist in the mold, and the lower recirculation still presents at the mold outlet. Therefore, the model height is set to 2.1 m to avoid treating backflow in the mold outlet directly otherwise and to gain insight into the lower recirculation.

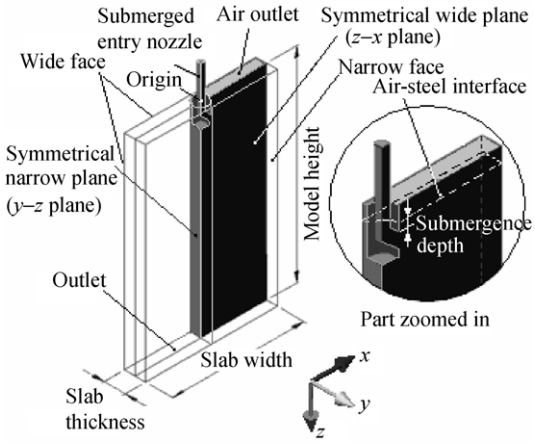

Fig. 1. Schematic model of the slab mold.

The equations that need to be solved in the model include continuity equation, momentum equation (with interface tension terms and momentum sink terms because of solidification), k-ε equations, and energy equations with solidification. All these equations are omitted in this simple article, and more information can be found in Refs. [9-13].

The following boundary conditions were applied along the computational domain.

(1) At the inlet of the SEN, a uniform normal velocity was specified according to the mass flow rate at the mold outlet and the turbulent parameters were calculated by semi-empirical formulae. In addition, casting temperature was given as the thermal boundary at the inlet.

(2) At the outlet of the model, the mass flow rate was consistent with that at the nozzle inlet and the normal gradient of other variables were assumed to be zero.

(3) Pressure was specified as constant and heat flux was set to be zero at the air outlet.

(4) For the narrow and wide symmetrical planes, the normal gradients of all variables were zero except the velocity perpendicular to the surface, which was assumed to be zero.

(5) No slip condition was applied to the narrow and

wide faces of the mold, and the slab was withdrawn with casting speed automatically when the molten steel solidified. The average heat transfer coefficients between mold walls and the surrounding were specified respectively. Other walls were supposed to be adiabatic.

The thermo-physical parameters of molten steel and air are summarized in Table 2 [8, 14].

Table 2. Physical parameters of molten steel and air

Steel density	7020 kg/m^3
Steel viscosity	0.0055 kg/(m·s)
Steel thermal conductivity	46.4 W/(m·°C)
Steel specific heat capacity	628 J/(kg·°C)
Steel latent heat of fusion	268 kJ/kg
Liquidus temperature	1514°C
Solidus temperature	1490°C
Air density	1.225 kg/m^3
Air viscosity	1.789×10^{-5} kg/(m·s)
Air thermal conductivity	0.024 W/(m·°C)
Air specific heat capacity	1006 J/(kg·°C)

3. Results and discussion

3.1. Flow and temperature fields in the mold

A strong jet is formed after the molten steel goes out of the nozzle port, which causes two big recirculations in opposite directions when it reaches the narrow face. Fig. 2 shows the velocity vector fields (left half) and isolines (right half) on the symmetrical *z*-*x* plane. For the case with the casting speed of 1.0 m/min, the mean velocity is 2.0 m/s at the nozzle inlet and larger than 1.0 m/s at the nozzle port outlet. The jet velocity decreases to 0.2-0.3 m/s when reaching the narrow face, which causes an impact on the inner shell face. The bigger recirculation at the lower part of the mold exceeds the domain of the mold outlet obviously, while the upper recirculation in the smaller zone with larger intensity results in a bad surface fluctuation. The curved face where the steel volume fraction equals 0.5 is set as the steel-air interface in the VOF model. According to this, taking the mean surface height (z=0.13 m) as the reference, Fig. 3 depicts the wave and velocity on the air-steel interface of the symmetrical *z*-*x* plane. It is observed that there are obvious wave crest and trough on the free surface. In this case, the wave crest is 50 mm away from the narrow face, and the trough is 400 mm away from the centerline of the nozzle, and the maximal wave height (MWH) defined as the height difference between the wave crest and trough is 6.9 mm. The surface velocity of the molten steel is corresponding with the wave height. The maximal surface velocity of 0.31 m/s occurs near the trough. In this operating condition, it is detrimental for controlling surface wave and reducing inclusions entrainment as well as defects.

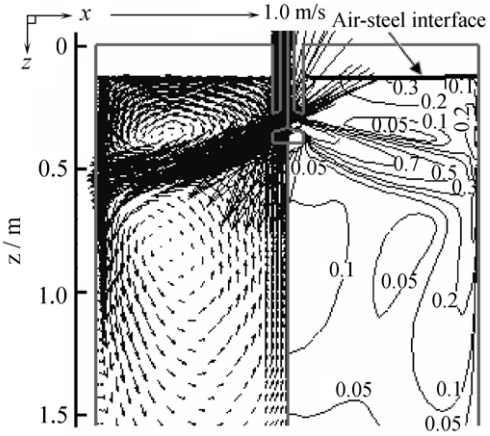

Fig. 2. Velocity distribution (m/s) on the symmetrical *z*-*x* plane.

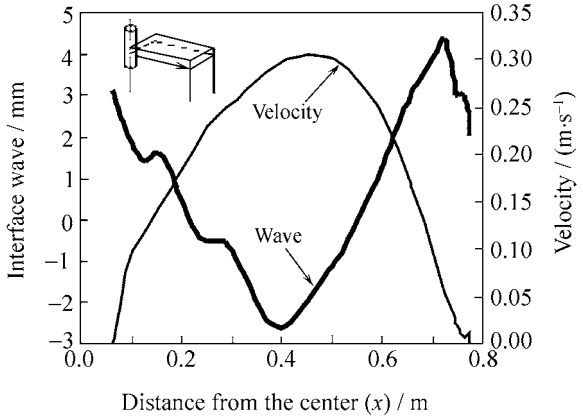

Fig. 3. Wave and velocity on the air-steel interface of the symmetrical *z*-*x* plane.

There is a close relationship between the heat transfer and flow pattern in the mold. Fig. 4 describes the isotherms on the symmetrical *z*-*x* plane, where the left and right halves show the molten steel's temperature and superheat, respectively. The molten steel with a temperature of 1540ºC from the nozzle port mixes with the surrounding liquid and heat convection takes place intensively. The isotherms are closer near the jet, which indicates that a sharp temperature drop presents there. The temperature of the jet decreases to about 1520°C when it reaches the narrow face. Totally, there is an obvious superheat of the molten steel near the impinging jet, and the superheat is below 5ºC elsewhere because of the intensive convection and turbulent dissipation. Concretely speaking, the isotherms go through the impingement point in two opposite directions. One goes downwards with a lower superheat of below 1ºC at most regions, while the other one moves towards the surface with a comparatively evident superheat of 1-4ºC.

Fig. 5 plots the isotherms on both wide and narrow shell surfaces. It seems that the isotherms on narrow

and wide shell faces look like the letters "W" and "V", respectively. When the jet impinges against the narrow face, it spreads towards the two wide faces quickly and causes heavy impact near the corners of the wide faces, where the molten steel cannot be cooled in time because of the relatively larger velocity. Therefore, the shell temperature there is higher than that at other places with the same height, resulting in isotherms with "W" profile at wide faces. Similarly, the velocity of the molten steel near the narrow face decreases from the center to the corner, and therefore, the isotherms look like the letter "V". Moreover, for the same temperature the isotherms at the narrow face move downward comparing with that at the wide face because of the stronger impingement at the narrow face. The isotherm distribution that depends on the flow pattern decides the shell thickness distribution directly, which will be illustrated later. In addition, the isotherms become sparser when the distance from the air-steel interface increases, which indicates that the temperature-drop speed is slowed down because of the fast decreasing heat flux on the shell surface in the height direction.

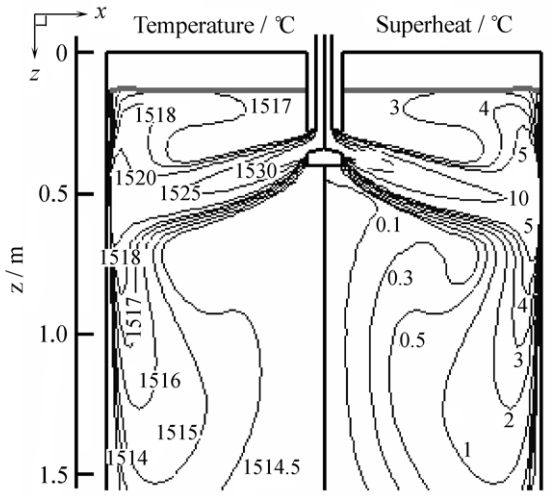

Fig. 4. Temperature and superheat distributions on the symmetrical *z*-*x* plane.

3.2. Shell thickness profile in the mold

Research on the shell thickness distribution is important to analyze the possibility of breakout and the place where breakout occurs and where cooling should be enhanced. Both shell thickness and temperature profiles on the centerlines of narrow and wide faces are shown in Fig. 6. The shell thickness on the wide face increases approximately linearly with the distance from the meniscus. However, on the narrow face, the two opposite-direction flows along the narrow faces near the impingement point erode the shell and prevent the shell growth, so that there are two zero-increase steps of shell thickness in a certain range near the impingement point (0.2-0.6 m from the meniscus). Fig. 7 depicts the relationship between the shell thickness at the centerline of the narrow face (x=0.775 m, y=0 m) and the impinging velocity on a vertical line (x=0.760 m, y=0 m) nearby the centerline, where the x-velocity component perpendicular to the narrow face is defined as the impinging velocity. It is clear that in the range of 0.2-m to 0.6-m distance from that meniscus, the x-velocity of molten steel is relatively larger. The so-called impingement point with the maximal x-velocity of 0.08 m/s is 0.36 m away from the meniscus. Therefore, near the impingement point (0.2-0.6 m from the meniscus), the shell thickness is lesser without increase. Especially, the thickness is only 4.8 mm at the impingement point. From Fig. 6, it can also be seen that the temperature profiles on the centerlines of narrow and wide faces have similar characteristics with the shell thickness profiles. In sum, the thin shell at the impingement point is prone to breakout for this case.

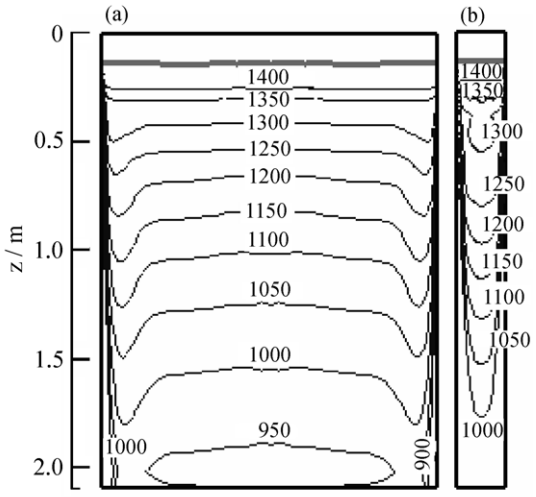

Fig. 5. Temperature distribution (°C) of the shell surface: (a) wide face; (b) narrow face.

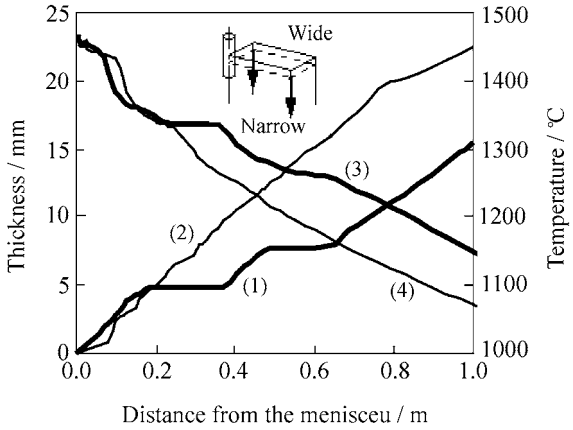

Fig. 6. Shell thickness and temperature profiles on the centerlines of narrow and wide faces: (1), (3) on narrow face; (2), (4) on wide face; (1), (2) for shell thickness; (3), (4) for shell temperature.

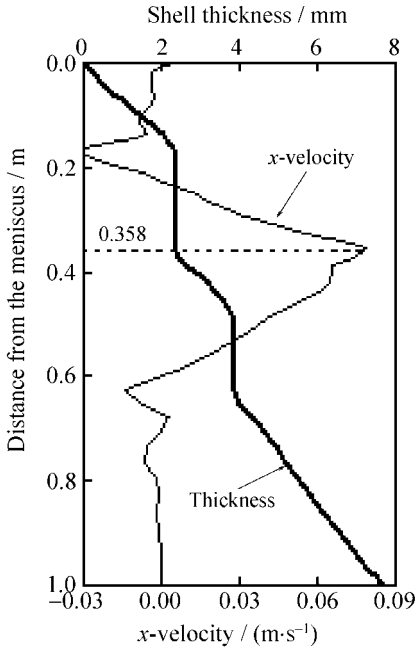

Fig. 7. Relationship between the shell thickness and impinging velocity on the centerline of the narrow face.

It is observed from Fig. 6 that the shell thicknesses of the centers of narrow and wide sides at the mold outlet cross-section are 13.1 and 21.0 mm, respectively, which indicate the uneven thickness distribution at the slab cross-section. The shell thickness around the sides of the slab cross-sections is shown in Fig. 8. The temperature and steel state distribution at the mold outlet are given in Fig. 8(a), where only half of the cross-section is shown because of the symmetry, and the three zones with the color from light to dark represent liquid, mushy, and solid steel. According to this, Fig. 8(b) plots the curves of the shell thickness varied with the length along shell sides. Two horizontal cross-sections, the mold outlet (z=0.9 m) and the one which the impingement point is on (z=0.488 m), are chosen. One quarter of the cross-section perimeter (width/2+thickness/2) and the shell thickness are set as x- and y-axes respectively in the above figure. The shell thickness is defined as the perpendicular distance from the inner point to the side of the cross-section, excluding the points at the corner of the slab, so that the curves are broken near the corner. It can be concluded from the figure that the position with the least shell thickness lies in the center of the narrow side for both two cross-sections, and the shell thickness near the corner of the wide face is also rather less, because after reaching the narrow face, the impinging jet spreads towards the two wide faces quickly and erodes the shell there. This result is consistent with the "W" isotherms on the wide shell face in Fig. 5. In practice, there is a larger heat resistance at the corners because of the air-gap between the shell surface and the mold wall resulting from shell shrinking, so that the shell there is considerably thinner and easier to breakout.

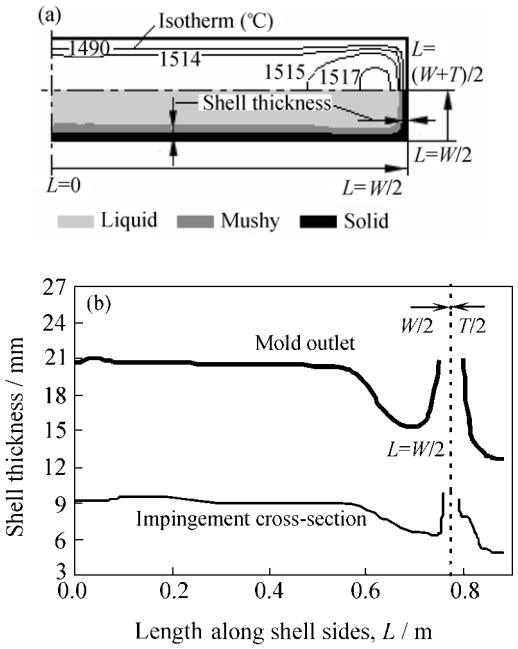

Fig. 8. Shell thickness around the sides of slab cross-sections: (a) temperature and steel state distribution at the mold outlet; (b) curves of shell thickness varied with the length along shell sides for the mold outlet and impingement cross-section.

3.3. Improvement

Based on the upper parts, we know that using the nozzle with a 15°-downward angle cannot increase the shell thickness effectively. The key to achieve this purpose is to decrease the jet impinging velocity, and thus, the nozzle design is very important. Investigating the streamline distribution inside the nozzles indicates that for a common nozzle, the steel flow with a high speed in the nozzle bore takes a big turning at the port, which brings in a recirculation flow at the upper portion of the nozzle port, as shown in Fig. 9(a). If defining the fraction of the outlet port area where the flow has a positive x component of velocity as the effective area fraction, then, this area fraction for common nozzle is 69%. The research results reveal that increasing both the port width and height can reduce this fraction; therefore, the jet velocity cannot be decreased in this way. According to the characteristics of the streamline inside the nozzle, the nozzle design is improved, as shown in Fig. 9(b). Comparing with the common one, the new nozzle with the same port outlet area has a 60°-downward angle at the upper face, and keeps the lower face angle as the same. The improved nozzle with roughly streamlined inner wall makes the flow fill the entire outlet and enhances the effective port area fraction to 100%. After optimization, the peak x-velocity at the vertical centerline of the port outlet changes from 1.8 to 1.2 m/s, decreasing one third.

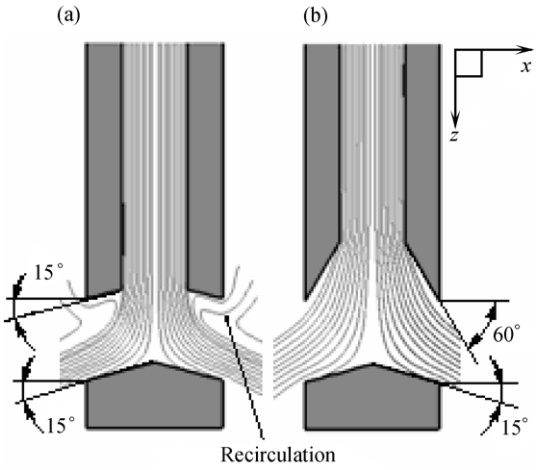

Fig. 9. Streamline distribution inside two nozzles: (a) common one; (b) improved one.

Fig. 10 compares the shell thickness profiles on the centerlines of both narrow and wide faces with the distance from meniscus for the common and improved nozzles. The difference of shell thicknesses on wide face for the two nozzles is slight, while the improved one can increase the thickness on the narrow face obviously, especially near the impingement point. The shell thickness there increases linearly with the increasing distance from the meniscus using the improved nozzle and such a shell thickness profile is desired to eliminate breakout. Fig. 11 plots the shell thickness around the sides of the slab cross-sections, which has the same meaning as Fig. 8. After optimization, the thicknesses are more uniform at the cross-sections, especially at the impingement cross-section, where the smallest shell thickness increases to 7.8 mm, namely, the increment of 63%, and the shell thickness at the center of the narrow face is nearly the same as that at the corner of the wide face on the impingement cross-section. Moreover, the shell thickness at the center of the narrow side on the mold outlet cross-section increases from 13.1 to 15.2 mm.

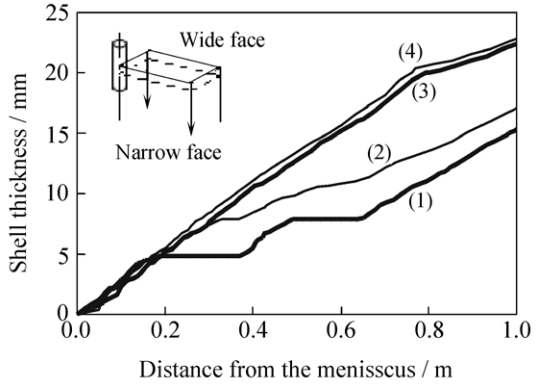

Fig. 10. Shell thickness profiles on the centerlines of narrow and wide faces: (1), (3) using common nozzle; (2), (4) using improved one; (1), (2) on the narrow face; (3), (4) on the wide face.

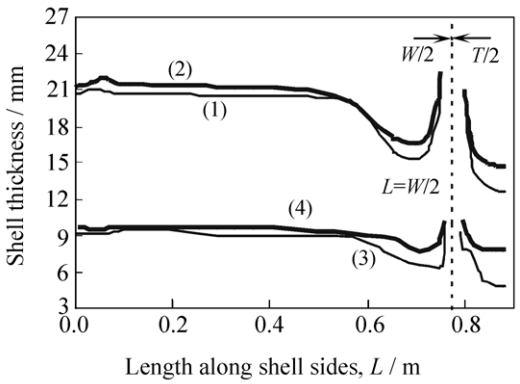

Fig. 11. Shell thickness around the sides of slab cross-sections: (1), (3) using the common nozzle; (2), (4) using the improved one; (1), (2) on the mold outlet cross-section; (3), (4) on the impingement cross-section.

In addition, the research shows that the new design can weaken the surface wave effectively. After improvement, the maximal wave height on the free surface decreases from 6.9 to 2.4 mm, and the peak surface velocity decreases from 0.31 to 0.19 m/s.

The calculation results were verified in certain steel plant where breakout took place at the narrow face and at the corners of the wide face for several times, and the modification with a new nozzle is under way.

4. Conclusions

(1) The temperature isotherms decided by the flow pattern, look like "W" and "V" on the wide and narrow shell surfaces, respectively, which indicate that the highest temperature locates at the center of the narrow face and on the wide face near the corner.

(2) The jet acts a stronger impingement on the shell of the narrow face, which causes a zero-increase of shell thickness in a certain range near the impingement point, while the shell thickness on the wide face increases approximately linearly with the increasing distance from the meniscus.

(3) The shell thickness is uneven on the slab cross-section, and the thinnest shell on the slab cross-section locates primarily at the center of the narrow face and secondly near the corner of the wide face.

(4) Increasing the port angle of the upper face to form a roughly streamlined inner wall can enhance the effective port outlet area evidently. The optimized nozzle can eliminate the recirculation at the upper portion of the nozzle port, reduce the velocity of the impinging jet, weaken the impact on the narrow shell face, increase the shell thickness of the narrow face, and especially make the shell thickness more uniform on the slab impingement cross-section.

References

[1] Z.Y. Zhu, X.H. Wang, W.J. Wang, and J.M. Zhang, Shell thickness distribution in mold and space between dendrites in the shell of continuous casting slab, *J. Univ. Sci. Technol. Beijing* (in Chinese), 22(2000), No.6, p.515.

[2] M.R. Aboutalebi, M. Hasan, and R.I.L. Guthrie, Coupled turbulent flow, heat, and solute transport in continuous casting processes, *Metall. Mater. Trans. B*, 26(1995), p.731.

[3] S.H. Seyedein and M. Hasan, A three-dimensional simulation of coupled turbulent flow and macroscopic solidification heat transfer for continuous slab casters, *Int. J. Heat Mass Transfer*, 40(1997), No.18, p.4405.

[4] C.B. Wu, Z.G. Li, and Q. Wang, Computer emulation of solidification behavior of molten steel in the mould of continuous caster, *Steelmaking* (in Chinese), 20(2004), No.3, p.44.

[5] L.G. Zhao and H. Zhang, Numerical studies on comprehensive metallurgical behaviors in continuous casting mold, *J. Iron Steel Res.* (in Chinese), 19(2007), No.5, p.29.

[6] Z.Q. Zhu, X.B. Yu, W.F. Gao, and Q.L. Shi, The study of water model research of SEN with rotational flow guide device, *Res. Iron Steel* (in Chinese), 34(2006), No.5, p.6.

[7] J.T. Huang and J.C. He, Numerical simulation of steel solidification and electromagnetic brake in the billet mold, *Acta Metall. Sin.* (in Chinese), 37(2001), No.3, p.281.

[8] M.Y. Ha, H.G. Lee, and S.H. Seong, Numerical simulation of three-dimensional flow, heat transfer, and solidification of steel in continuous casting mold with electromagnetic brake. *J. Mater. Process. Technol.*, 133(2003), p.322.

[9] C.W. Hirt and B.D. Nichols, Volume of fluid (VOF) method for the dynamics of free boundaries, *J. Comput. Phys.*, 39(1981), p.201.

[10] B.E. Launder and D.B. Spalding, Numerical computation of turbulent flows, *Comput. Methods Appl. Mech. Eng.*, 3(1974), p.269.

[11] B.G. Thomas, Q. Yuan, S. Sivaramakrishnan, T. Shi, S.P. Vanka, and M.B. Assar, Comparison of four methods to evaluate fluid velocities in a continuous slab casting mold, *ISIJ Int.*, 41(2001), No.10, p.1262.

[12] V.R. Voller and C.R. Swaminathan, Source-based method for solidification phase change, *Numer. Heat Transfer B*, 19(1991), p.175.

[13] V.R. Voller and C. Prakash, A fixed-grid numerical modeling methodology for convection-diffusion mushy region phase-change problems, *Int. J. Heat Mass Transfer*, 30(1987), p.1709.

[14] Q. Li, J.J. Wang, and Li Zhou, Simulation on fluid flow and solidification coupled analysis in beam blank continuous casting mould, *J. Anhui Univ. Technol.* (in Chinese), 24(2007), No.1, p.18.